SIAM J. Applied Dynamical Systems
Vol. 1, No. 1, pp. 146–174

Synchronized Activity and Loss of Synchrony Among Heterogeneous Conditional Oscillators*

Jonathan Rubin† and David Terman‡

Abstract. The inspiratory phase of the respiratory rhythm involves the synchronized bursting of a network of neurons in the brain stem. This paper considers activity patterns in a reduced model for this network, namely, a system of conductance-based ordinary differential equations with excitatory synaptic coupling, incorporating heterogeneities across cells. The model cells are relaxation oscillators; that is, no spikes are included. In the continuum limit, under assumptions based on the disparate time scales in the model, we derive consistency conditions sufficient to give tightly synchronized oscillations; when these hold, we solve a fixed point equation to find a unique synchronized periodic solution. This solution is stable within a certain solution class, and we provide a general sufficient condition for its stability. Allowing oscillations that are less cohesive but still synchronized, we derive an ordinary differential equation boundary value problem that we solve numerically to find a corresponding periodic solution. These results help explain how heterogeneities among synaptically coupled oscillators can enhance the tendency toward synchronization of their activity. Finally, we consider conditions for synchrony to break down.

Key words. oscillations, synchrony, synaptic coupling, heterogeneity, respiratory rhythm

AMS subject classifications. 34C15, 34C26, 37C25, 45J05, 92C20

PII. S111111110240323X

1. Introduction.

The inspiratory phase of the respiratory rhythm may originate in a network of interacting cells in a region of the brain stem called the pre-Bötzinger complex (pre-BötC) [17]. Within the pre-BötC, when coupling among cells is blocked, there are silent cells, cells that spike repeatedly, and intrinsically bursting cells that generate groups of spikes separated by pauses [12, 14, 17]. The burst frequencies vary among different bursting cells, depending on differences both in intrinsic cell properties and in inputs to the cells from other brain regions. Moreover, cells in all groups seem to be capable of bursting, if provided with appropriate inputs experimentally; hence they are referred to as conditional pacemakers.

Experiments in brain slices have shown that a coupled network of pre-BötC cells typically displays synchronized bursting oscillations, even though some uncoupled cells are silent or repeatedly spiking. Indeed, simulations suggest that with only about 10% of the cells in the network operating in the intrinsic bursting mode when uncoupled, a model pre-BötC network can still generate a synchronized population rhythm [3, 6]. Within the synchronized

*Received by the editors February 27, 2002; accepted for publication (in revised form) by T. Kaper July 23, 2002; published electronically August 2, 2002.
http://www.siam.org/journals/siads/1-1/40323.html
†Department of Mathematics and Center for the Neural Basis of Cognition, University of Pittsburgh, Pittsburgh, PA 15260 (rubin@math.pitt.edu). The work of this author was partially supported by NSF grants DMS-9804447 and DMS-0108857.
‡Department of Mathematics, Ohio State University, Columbus, OH 43210 (terman@math.ohio-state.edu). The work of this author was partially supported by NSF grant DMS-0103822.

cell population, details of the bursting pattern, such as precise onset and offset times, may differ slightly from cell to cell, presumably relating to the presence of intrinsic and input heterogeneities. Synchronization can also break down as it is replaced by a more complex bursting pattern such as a 2:1 or 4:1 rhythm, in which some subset of cells joins in only on 1 out of every 2 or 4 bursts of the rest of the cells [3], or perhaps even chaos [7].

In two papers, Butera and collaborators presented simulation results for models for individual cells in the pre-BötC [2] as well as for a network composed of these cells [3]. In the network, only excitatory coupling was included, as synchronized respiratory rhythms in pre-BötC persist under experimental blockage of inhibition but not under blockage of excitation [14]. For the most part, each cell was coupled to all other cells, since qualitatively similar results were found for sparse and full connectivities [3]. Cells also received tonic external excitatory input, with input strengths varying across the population.

The simulations in [2] captured the fact that individual neurons in the pre-BötC can be transformed from silent to bursting to repeated spiking states by varying certain parameters. When coupled, the simulated cells tended to engage in synchronized oscillations. Interestingly, while coupling among identical cells increased the range of external input levels over which synchronized oscillations occurred, relative to the oscillatory range for a single cell, networks of coupled cells with *heterogeneities* in certain parameter values displayed the broadest such dynamic range [3]. Thus heterogeneities in intrinsic cellular parameters and in external input levels are hypothesized to play key roles in enhancing the robustness of the respiratory rhythm and in shaping the details of cellular activity during these oscillations.

In this paper, we consider a synaptically coupled network of pre-BötC pacemaker cells, each featuring heterogeneities in certain parameters, with each cell governed by a reduced version of the conductance-based neuronal model presented in [2]; the model is introduced in section 2. We treat this system via both simulation and analysis. We perform simulations on a network of 20 heterogeneous cells with all-to-all excitatory synaptic coupling, with results presented in section 3. Our simulations, done with XPPAUT (developed by G. B. Ermentrout [8] and available at http://www.math.pitt.edu/~bard/xpp/xpp.html), provide a useful tool for phase space visualization of dynamics of nonidentical coupled oscillators. In particular, in animations of our results, we display nullclines, which dynamically evolve according to coupling levels present. For these nullclines, we also show the corresponding curves of knees, as defined in section 2, which evolve similarly. For oscillatory dynamics, the curves of knees are crucial in determining which cells are able to oscillate on each cycle of network activity, and the visualization that we provide gives an extremely clear way to view their role while network activity is in progress.

For our analytical treatment, we work in the continuum limit, in which the number of cells in the population is infinite. Our results thus yield a good approximation of network behavior with large numbers of cells, which is the biologically realistic scenario but for which direct simulations become difficult. Our analysis, in sections 4 and 5, provides conditions for the existence of stable synchronized relaxation oscillations in a reduced pre-BötC model. When these conditions are satisfied, all cells in the network will begin and terminate their active phases together, although they will do so from a distribution of voltage levels. Our analysis shows that, when it exists, this synchronized oscillatory solution is unique. It also yields a formula that pinpoints the location of cells at onset of activity, in an appropriate

phase space. We prove that this solution is always stable within a certain solution class, and we provide a general sufficient condition for its stability. Alternatively, for the case of a more gradual onset of activity, observed in our simulations and in [3] for some parameter values, we derive in section 6 an ordinary differential equation boundary value problem that can be solved numerically for the location of the cells at activity onset (or termination). The same approach can be used to give conditions for synchrony with a gradual termination of activity. Finally, in section 7, we give a condition under which a cell configuration in phase space will not generate a synchronized oscillation, and we conclude with a discussion in section 8.

Synchronization of coupled oscillators has received significant attention in past works. In particular, synchrony is one of many activity patterns considered previously in modeling studies of networks of synaptically coupled relaxation oscillators (reviewed in [13, 16]). A novel feature of this paper is the inclusion of the effects of heterogeneity in such a network (see also [10, 19, 20, 5]). Heterogeneity has been found previously to compromise the robustness of synchronization in networks of *spiking* neurons with inhibitory coupling [4, 21]. Our analysis explains how heterogeneity can actually promote synchrony in a network of relaxation oscillators with excitatory synaptic coupling, even when some cells in the network would be unable to oscillate in isolation or with synaptic input only from cells identical to them. Similar mechanisms are likely to act to promote synchrony in heterogeneous populations of *bursting* neurons.

2. Model.

2.1. Single cell.

We model each cell by a system of ordinary differential equations of the form

$$\begin{aligned} v' &= f(v,h) + I_{app} + I_{syn}, \\ h' &= \epsilon g(v,h). \end{aligned} \tag{2.1}$$

Here $v(t)$ represents the membrane potential of the cell, and h is a channel state variable, as described below. The parameter I_{app} denotes an applied current, and $\epsilon > 0$ is assumed to be a small, singular perturbation parameter. The term I_{syn} encompasses coupling from other cells; it is described in detail below.

Suppose, for now, that $I_{syn} = 0$. We assume that the v-nullclines $\{f(v,h) + I_{app} = 0\}$ are cubic-shaped for all values of I_{app} of interest. Moreover, the h-nullcline $\{g(v,h) = 0\}$ is a monotone decreasing curve that intersects each of the v-nullclines at a single point, denoted by $p_0 = p_0(I_{app})$; see Figure 1. We further assume that $v' > 0$ (< 0) above (below) the v-nullcline and $h' > 0$ (< 0) below (above) the h-nullcline. It follows that, if p_0 lies on the middle branch of the v-nullcline, then (1) exhibits a stable limit cycle for all ϵ sufficiently small, while, if p_0 lies on either the left or right branch of the cubic nullcline, then p_0 is a globally stable fixed point for all ϵ sufficiently small.

In the simulations that follow, we consider a specific instance of (2.1), namely, the conductance-based model

$$\begin{aligned} C_m v' &= -g_{Na} m_\infty(v) h (v - v_{Na}) - g_L (v - v_L) + I_{syn} + I_{app}, \\ h' &= (h_\infty(v) - h)/\tau_h(v), \end{aligned} \tag{2.2}$$

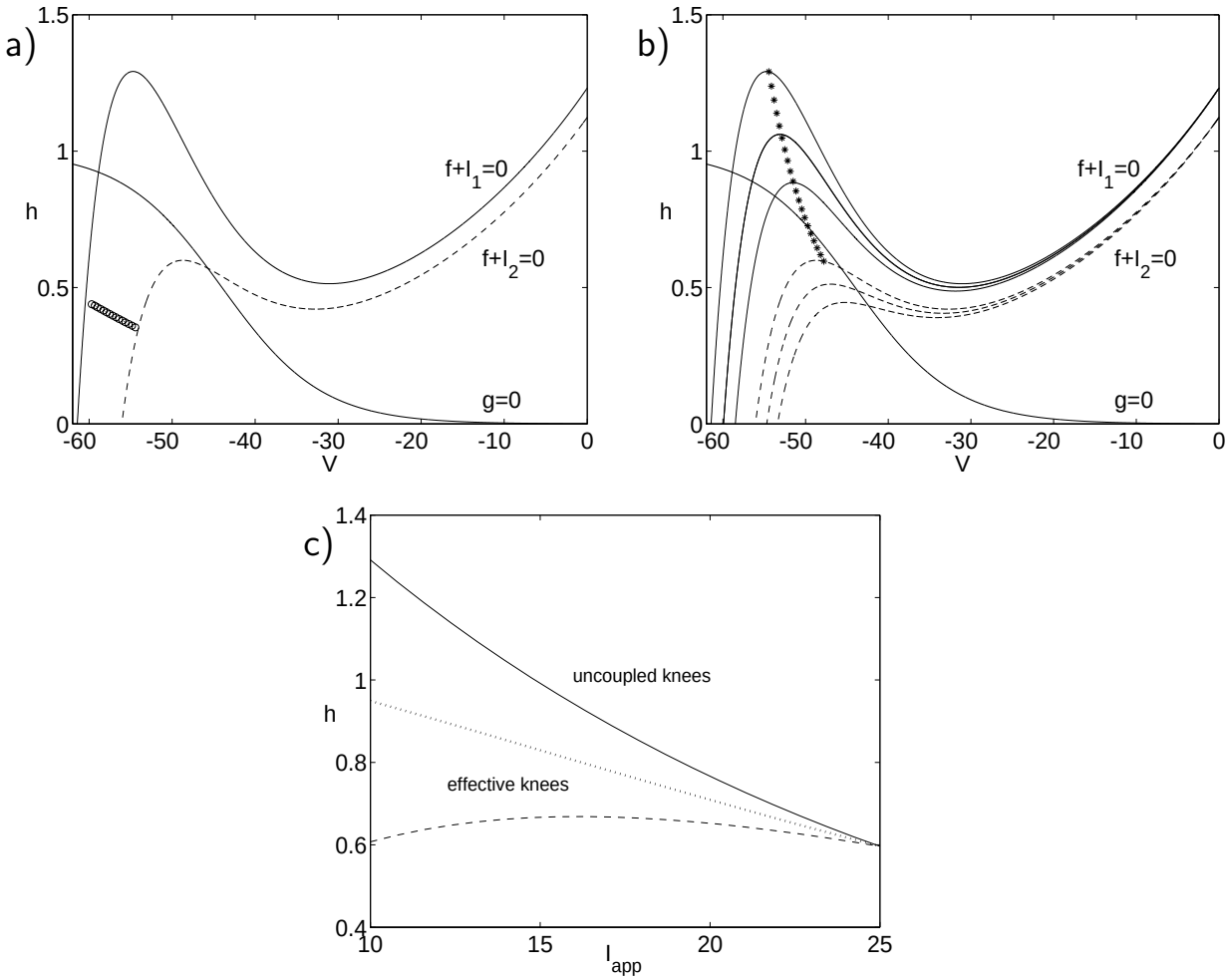

Figure 1. *Numerically generated nullclines for* (2.2) *in the* (v, h)*-phase plane, with parameters from the appendix.* (a) *Increasing excitatory input* $I_{app} > 0$ *(from* $I_1 = 10$ *to* $I_2 = 25$*) lowers the* v*-nullcline (here* $I_{syn} = 0$*). Cells with a range of* I_{app} *values can all be visualized in the same phase plane; an example representing the position of* 15 *cells is shown by the dark curve of circles.* (b) *Excitatory synaptic inputs further lower nullclines for* $v < v_{syn}$*. The dark curve denoted by asterisks gives a numerical approximation to the left curve of knees for* $I_{syn} = 0$ *and for* I_{app} *ranging from* I_1 *up to* I_2*.* (c) *Uncoupled* $(h_{LK}(I_{app}))$ *and effective left knees. The solid curve shows the left knee curve from part* (b)*. The other curves show effective knees computed numerically for* $g_{syn}/N = .005$ *(dotted) and* $g_{syn}/N = .01$ *(dashed) with* I_{syn} *computed by assuming that cells jump up to the active phase in order of decreasing* I_{app}*. Larger* g_{syn} *lowers the effective knees, promoting synchrony.*

where h_∞, m_∞ are monotone decreasing and increasing sigmoidal functions, respectively. The full functional forms and parameter values used are given in the appendix; these are based on models in [2, 3] but with sodium and potassium spiking currents blocked. The first equation in (2.2) describes the evolution of the voltage across a cell's membrane, with capacitance C_m, in terms of a persistent sodium current (I_{NaP} in [2, 3]), a leak current, and input currents. The second equation describes the slow inactivation of the persistent sodium current. For

biophysically relevant parameter values, (2.2) can be considered as singularly perturbed, since h evolves much more slowly than v.

The v-nullclines of (2.2) for different values of I_{app}, with $I_{syn} = 0$, are shown in Figure 1a, along with the h-nullcline. On each nullcline, the left branch corresponds to the *silent phase*, where a neuron fires no spikes, and the right branch corresponds to the *active phase*, where a neuron is said to be spiking. For all values of I_{app} considered, the v-nullcline has two saddle-node points, or knees, where the branches coalesce; see Figure 1b–c. We refer to these as a left knee at a smaller value of v and a right knee at a larger value; we denote the left curve of knees by $(v_{LK}, h_{LK})(I_{app})$ and the right curve by $(v_{RK}, h_{RK})(I_{app})$. Let I_{max} denote the maximum of the values of I_{app} over the cell population, and set $h_{LK} = h_{LK}(I_{max})$.

Note from (2.2) that increasing I_{app} lowers the v-nullclines. If I_{app} is sufficiently small, then the fixed point p_0 lies on the left branch of the v-nullcline, and the system is said to be excitable. For larger values of I_{app}, the fixed point lies on the middle branch of the cubic nullcline, and the system is oscillatory, with a periodic solution that jumps up from the silent phase to the active phase and then down from the active phase to the silent phase. Thus this system captures the conditional pacemaker property of pre-BötC cells.

Simulations in [3] show that the biological effects of heterogeneities among cells in the pre-BötC are reproduced by introducing heterogeneities in the applied current I_{app} and in the intrinsic parameters v_L and g_{Na} in (2.2). The influences of heterogeneities in I_{app} and v_L in (2.2) can be combined by defining a new parameter $\tilde{I}_{app} = g_L v_L + I_{app}$. For notational convenience, we will instead, without loss of generality, fix $g_L v_L$ and restrict variations to I_{app}. In this paper, we will focus on heterogeneities in I_{app}, although we mention specific influences of heterogeneities in g_{Na} in the discussion.

2.2. Synaptic coupling. We now describe I_{syn}, the coupling between cells. First, consider a population of N discrete cells, and let the coupling to cell j be given by

$$I_{syn} = \frac{g_{syn}}{N}\left(\sum_{k=1}^{N} s_\infty(v_k)\right)(v_{syn} - v_j), \tag{2.3}$$

where

$$s_\infty(v) = 1/(1 + \exp((v - \theta_s)/\sigma_s)).$$

Here we are assuming that the coupling is all-to-all and homogeneous. (That is, the form of s_∞ does not depend on the index k.) Note that, if σ_s is very small, then $s_\infty(v) \approx H(v - \theta_s)$, where H is the Heaviside step function; that is, $s_\infty(v) \approx 0$ if $v < \theta_s$, and $s_\infty(v) \approx 1$ if $v > \theta_s$. In the analysis, we assume that $s_\infty(v) = H(v - \theta_s)$. The value θ_s is such that a cell's voltage increases through θ_s as it jumps up to the active phase.

In (2.3), $g_{syn} > 0$ represents the maximal synaptic conductance, and v_{syn} is the synaptic reversal potential. We will choose v_{syn} so that $v_k(t) < v_{syn}$ for each k along every solution of interest. This implies that I_{syn} is always positive, corresponding to excitatory coupling; see Figure 1b.

In the analysis, we will consider the continuum limit of infinitely many cells. We assume that each cell is parameterized by a point x in some domain D. One may view D as some subset of $\mathbb{R}^3$; however, this is not necessary. We then denote the dependent variables as

$v(x,t)$ and $h(x,t)$. As before, heterogeneities will be in the applied currents, which we denote as $I_{app}(x)$. We then let

$$I_{syn}(x,t) \;=\; (g_{syn}/Vol)\,(v_{syn}-v(x,t))\int_D s_\infty(v(x,t))dx, \tag{2.4}$$

where s_∞ is defined as above and $Vol=\int_D dx$.

When $I_{syn}=0$, the h-values $h_{LK}(I_{app}), h_{RK}(I_{app})$ for the knees of the v-nullcline are defined by solving the two equations $f+I_{app}=0$ and $\partial f/\partial v=0$. Suppose that all cells with the same value of I_{app} are synchronized, such that the parameterization by x is equivalent to a parameterization by I_{app}. For $I_{syn}>0$ given by (2.4), the equations $f+I_{syn}+I_{app}=0$ and $\partial(f+I_{syn})/\partial v=0$ then define curves $h(I_{app})$ as well. When solutions exist, we refer to these as *effective knees*. The effective knees will be crucial for determining which cells jump up to the active phase in a network oscillation. An example appears in Figure 1c, based on the assumption that cells jump up to the active phase in order of decreasing I_{app}, such that I_{syn} becomes larger for cells with smaller I_{app}. The role of the effective knees is illustrated in the numerical simulations in the next section. Note that, in Figure 1c, the effective curve of knees may be nonmonotone due to the larger value of I_{syn} that occurs for smaller I_{app} when cells jump up to the active phase in order of decreasing I_{app}.

3. Numerical simulations of network activity. In this section, we present numerical simulations of (2.2) that illustrate different population rhythms exhibited by the model network. We consider a population of 20 cells and denote the dependent variables corresponding to cell i, $1\le i\le 20$, as $(v_i(t),h_i(t))$. We assume that the heterogeneity parameter I^i_{app} varies in a uniform linear fashion between $I_{min}=10$ and $I_{max}=25$. Note that, when $I_{app}=I_{min}$, system (2.2) with $I_{syn}=0$ is excitable, while, if $I_{app}=I_{max}$, then (2.2) is oscillatory. We demonstrate how the population rhythm changes as we vary the parameter $\bar g_{syn}=g_{syn}/20$.

First suppose that $\bar g_{syn}=.012$. Then the cells' activities are fairly well synchronized. This is demonstrated in Figure 2a, where we show the evolution of each $v_i(t)$. Note that all of the cells jump up to and down from the active phase at approximately the same times. Further, ordered jumping up occurs, such that cells with larger values of I_{app} jump up before cells with smaller I_{app}, as seen in the simulations in [3].

Perhaps a more illuminating way to present this solution is presented in Figure 3. This shows the evolution of each $(v_i(t),h_i(t))$ in the same (v,h) phase plane, along with the cubic-shaped v-nullclines (in black for ilow $\equiv I_{min}$ and in red for ihigh $\equiv I_{max}$) and effective knees corresponding to different levels of applied current and synaptic coupling. The synaptic coupling level is displayed in the upper-right corner as s_{tot}, defined as $\sum_{k=1}^{20} s_\infty(v_k)$. Cells are color-coded according to their I_{app} values, with red for largest I_{app} and dark blue for smallest I_{app}, and the effective left and right knees for each cell share its coloring. As s_{tot} changes, the effective knee positions move correspondingly. From this animation, we can observe that the cell with largest I_{app} jumps up first. Moreover, since the excitatory coupling lowers the nullclines and corresponding knees for cells while any cells are in the active phase, we see that synaptic coupling here prolongs active phases and slows oscillation frequency relative to the uncoupled case (as a consequence of fast threshold modulation; see [18]). This is similar, but complementary, to the mechanism by which inhibition can speed up rebound burst frequency

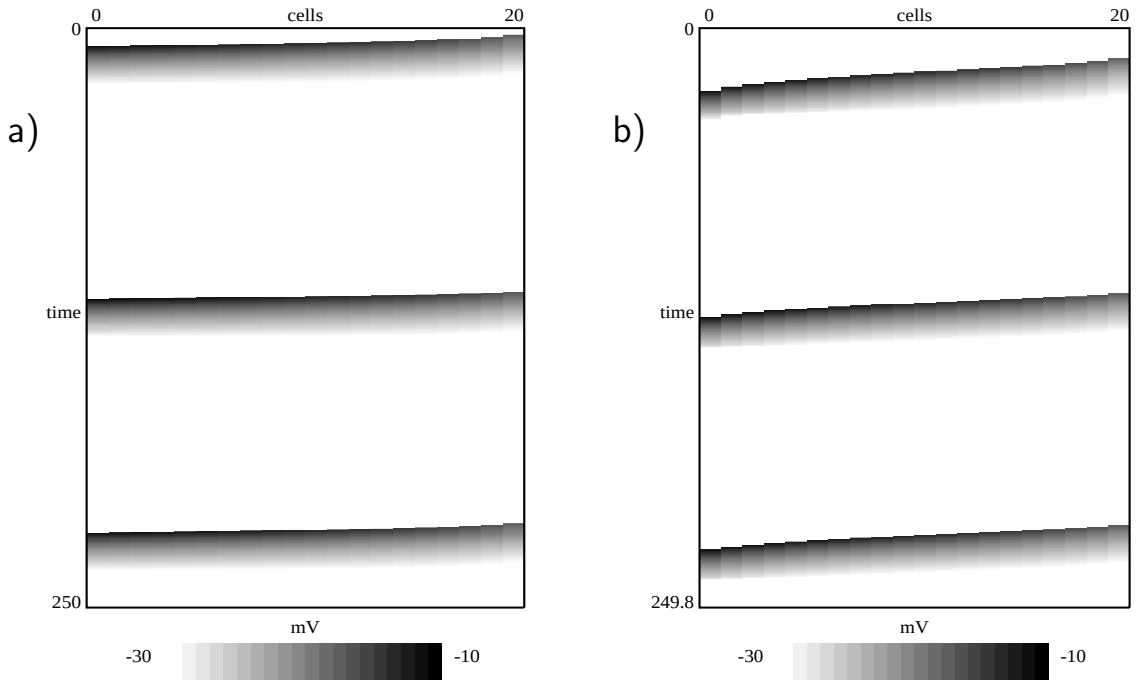

Figure 2. *Voltage versus time for synchronized oscillations of* 20 *heterogeneous pre-BötC cells. Moving horizontally across the figure corresponds to picking out different cells in the network. Time evolves downward. Voltage is coded in greyscale. The range of voltages encoded is limited to* $-30mV$ *up to* $-10mV$ *in order to focus sharply on the active phases of oscillations, which correspond to the dark bands in the figure. Cells with larger* I_{app} *values are labelled by higher numbers, appearing to the right in the figure. Note that cells with large* I_{app} *tend to jump up earliest in each cycle.* (a) $\bar{g}_{syn} = 0.012$ *gives a fairly unified jump-up.* (b) $\bar{g}_{syn} = 0.009$ *gives a more gradual jump-up.*

in networks [11], and it agrees with the observation in [3] that excitatory synaptic coupling slows oscillation frequency.

Figure 3 clearly demonstrates that each cell, while in the silent (active) phase, lies along the left (right) branch of the cubic corresponding to the level of applied current and synaptic input it is receiving. The positions of all of the cells at each fixed time approximates a curve that evolves in the (v, h) phase plane. We refer to this curve as a *snake of synchrony*. The primary goals of this paper are to derive conditions for when such a synchronous solution exists and to derive an analytic expression for the corresponding evolving snake curve.

Remark 3.1. Generally, a synchronous solution can be defined as one in which all cells jump up to the active phase on each cycle, and no active cell jumps down until all cells have jumped up. In our analysis, we will consider different types of synchronous solutions. In one, cells will jump up at the same moment in time, in an appropriate sense. In another, we allow cells to jump up at different times, but we require that no active cell jumps down until all of the other cells are active. In both cases, we assume that cells with $I_{app} = I_{max}$ jump up first and that cells jump up in order of decreasing I_{app}, as observed in simulations.

As we gradually decrease g_{syn}, and thus $\bar{g}_{syn}$, different cells may jump down first, and then the jump-up may become less unified (Figures 2b and 4). Note from Figure 2b and

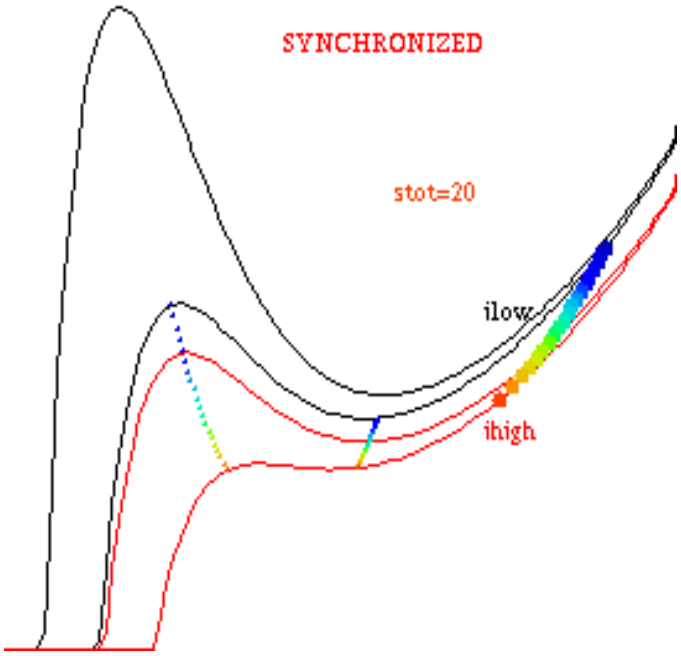

Figure 3. *Animation of a simulated synchronized oscillation with unified jumps ($\bar{g}_{syn} = .012$). Since all cells jump up at similar times, they end up fairly close together in the active phase, as shown in this still frame. Since all cells are in the active phase in the still frame, $s_{tot} = \sum_{k=1}^{20} s_\infty(v_k) = 20$.*

Figure 4 that the same cell (with $I = I_{max}$) jumps up and down first; as g_{syn} is weakened and the jump-up becomes more gradual, cells become unable to catch up to the lead cell with $I = I_{max}$ in the active phase. Finally, for still smaller g_{syn}, synchrony is lost, and more exotic population behaviors arise. For example, suppose that $\bar{g}_{syn} = .00825$, and consider the solution shown in Figures 5a and 6. Note that the entire population breaks up into two groups. Cells within each group are fairly well synchronized; however, one of the groups jumps up to the active phase only during every second cycle of the other group. As we decrease g_{syn}, solutions become increasingly more complicated. Figures 5b and 7, for instance, show that, when $\bar{g}_{syn} = .0035$, the solution appears to be quite irregular and possibly chaotic. Moreover, cells with $I_{app} < I_{max}$ may now jump up first on certain cycles, as seen in Figure 7. This can happen because, when a cell fails to jump up on one cycle, it can end up quite close to its uncoupled knee in the silent phase after active cells jump down on that cycle. Finally, when g_{syn} is sufficiently small, cells behave essentially as if they are uncoupled.

4. Analysis of snakes—preliminaries.

4.1. Introduction. Here and in section 5, we derive an analytic expression for a periodic solution to (2.1), consisting of a snake of synchrony for which all cells become active on each cycle of network activity, and conditions for when such a solution exists. In order to derive the analytic formulas, it will be necessary to make several simplifying assumptions on the nonlinear functions in (2.1). These assumptions are based on the numerical simulations of

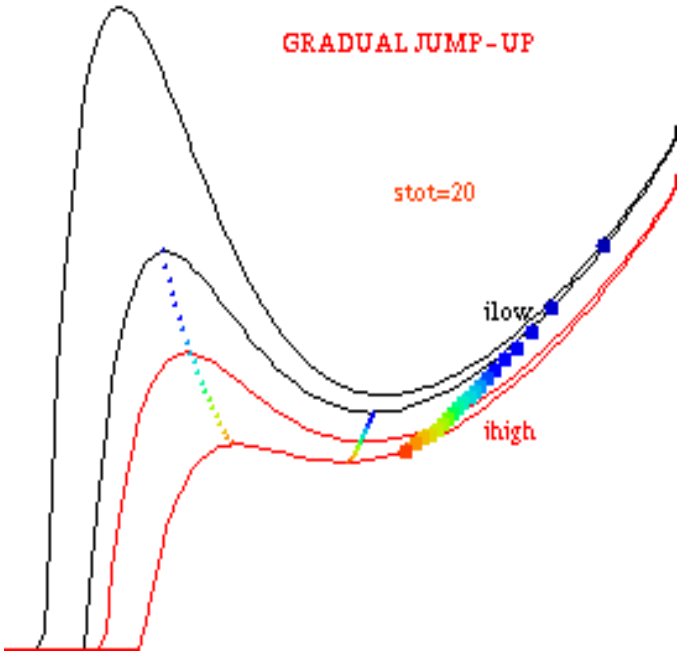

Figure 4. *Animation of a simulated synchronized oscillation with gradual jump-up ($\bar{g}_{syn} = .009$). The gradual jump-up causes cells to be quite spread out in the active phase, as shown in this still frame.*

(2.2) discussed above as well as the forms of the nonlinearities in (2.2), as discussed below and in the appendix. In particular, to derive explicit formulas, we assume that all cells jump up and down together, in a sense to be made precise below. This is quite accurate for large g_{syn}. In section 6, we allow for more gradual jumping. This does not lead to an explicit snake formula but rather to a single ordinary differential (with respect to I_{app}) equation boundary value problem that can be solved numerically for the periodic solution, expressed as a curve parameterized by I_{app}.

Recall that a snake of synchrony is a curve in the (v, h) phase plane, parameterized by the position $x \in D$, that evolves in time. For our analysis, it will be more convenient to parameterize the snakes by the heterogeneity parameter I_{app}, which we usually write as simply I. As noted earlier, this is justified if all of the cells with the same input I_{app} are completely synchronized; that is, if $I_{app}(x_1) = I_{app}(x_2)$, then $(v(x_1, t), h(x_1, t)) = (v(x_2, t), h(x_2, t))$ for all t. Under this assumption, we denote the snake as $(v(I, t), h(I, t))$ for $I_{min} \le I \le I_{max}$, where I_{min} and I_{max} are the minimum and maximum values of I_{app} for $x \in D$, respectively. (It is assumed that each of I_{min} and I_{max} is attained for some x in D, justifying the notation, and that both are finite.) We shall refer to either the cells with input I or the position in phase space of these cells as *cell(I)*.

We assume that, initially, the snake is in the silent phase with one of the cells at a left knee ready to jump up. This will turn out to be the cell (or cells) with the maximum applied current I_{max}, as discussed in the previous section and Remark 3.1. We then follow the snake around in phase space until it completes one cycle. This cycle consists of four pieces: the

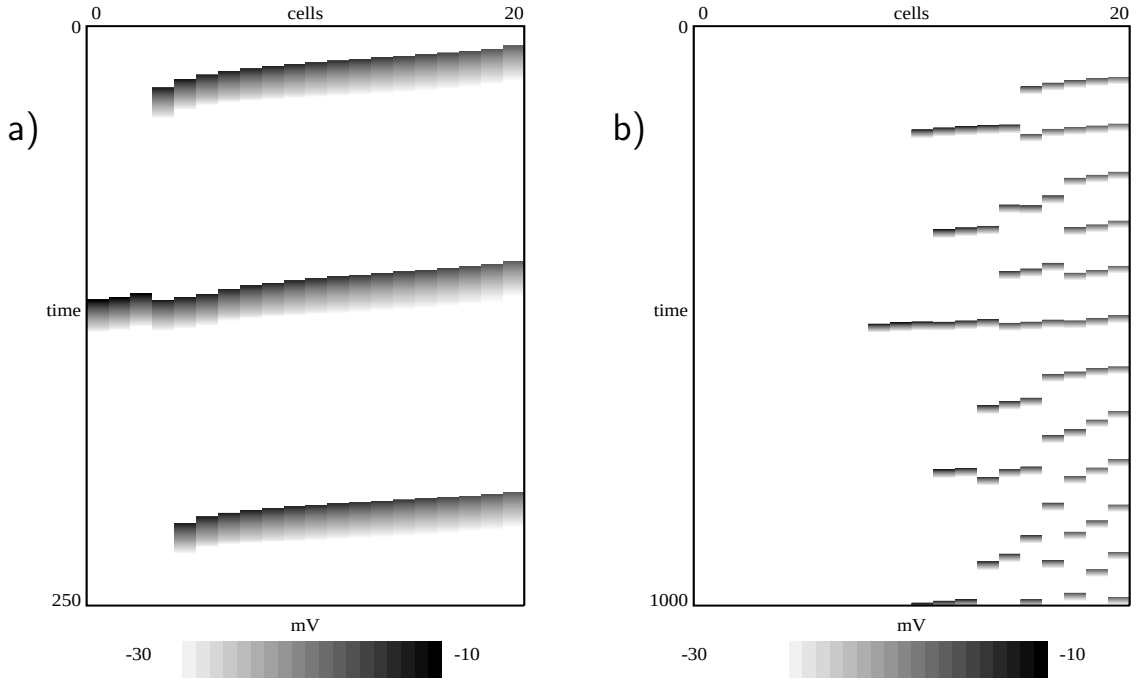

Figure 5. *Voltage versus time for asynchronous rhythms of* 20 *heterogeneous pre-BötC cells.* (a) *With* $\bar{g}_{syn} = .00825$*, three oscillation cycles are shown; in the first and third, several of the cells with small* I_{app} *fail to become active.* (b) *With* $\bar{g}_{syn} = .0035$*, participation in the oscillations is irregular, especially for cells on the edge of the participating and nonparticipating regions of the population.*

jump-up, the active phase, the jump-down, and the silent phase. We analyze the evolution of the snake over each of these pieces in the subsections below. The analytic formula for the snake is then obtained by assuming that the snake returns after one complete cycle to precisely the position from which it started. We derive the formula for the position of the snake at jump-up, although this could be done similarly for the snake position at other stages in a cycle.

4.2. The silent and active phases. We now derive equations for the evolution of the cells during the silent and active phases. The first step is to introduce the slow time scale $\tau = \epsilon t$ in (2.1). We then set $\epsilon = 0$ and $I_{tot}(x,t) = I_{app} + I_{syn}(x,t)$ to obtain the reduced equations

$$\begin{aligned} 0 &= f(v,h) + I_{tot}, \\ h' &= g(v,h), \end{aligned} \tag{4.1}$$

where differentiation is now with respect to τ. The first equation states that the cells lie along either the left or right branch of the cubic v-nullcline determined by I_{tot}; we refer to these nullclines simply as cubics below. We denote these branches as

$$v = v_L(h, I_{tot}) \quad \text{and} \quad v = v_R(h, I_{tot}),$$

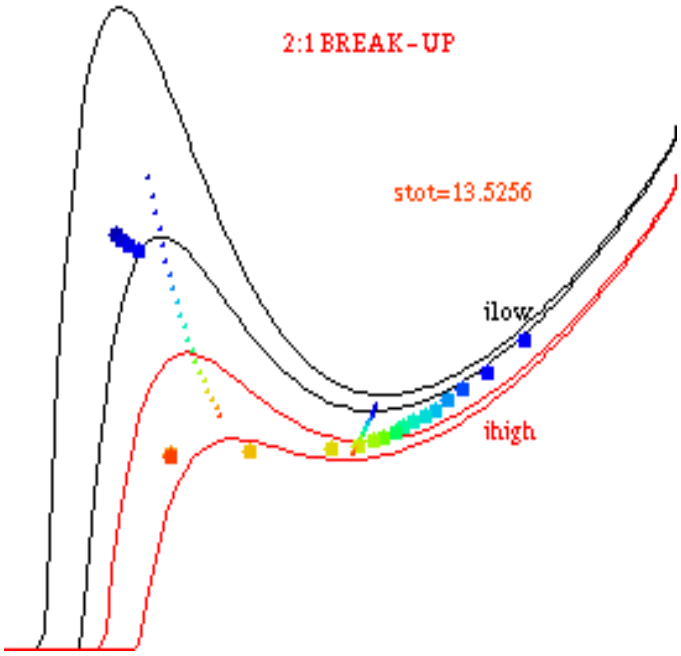

Figure 6. *Animation of a simulated solution that breaks up ($\bar{g}_{syn} = .00825$). This still frame shows the red and orange cells, with largest I_{app}, beginning to jump down, while the darkest blue cells, with smallest I_{app}, have failed to reach their effective knees for jump-up.*

respectively. Substituting this into the second equation of (4.1), we find that the slow variables h satisfy scalar equations of the form

$$h' = g(v_\alpha(h, I_{tot}), h) \equiv G_\alpha(h, I_{tot}), \tag{4.2}$$

where $\alpha = L$ or R depending on whether the cell lies in the silent or active phase, respectively.

We next make some simplifying assumptions on the nonlinear functions. These will allow us to solve the scalar equations (4.2) explicitly. We first consider the active phases, during which the cells lie along the right branches of certain cubics. For these values of (v, h), we assume that

$$h' = G_R(h, I_{tot}) = -\rho h \tag{4.3}$$

for some positive constant ρ. In order to justify this assumption, we consider the biophysical model (2.2), in which

$$g(v, h) = (h_\infty(v) - h)/\tau_h(v). \tag{4.4}$$

For the parameter values given in the appendix, one finds that $h_\infty(v)$ is extremely small and $\tau(v)$ is nearly constant while the cells are in their active phases. This then leads to the approximation (4.3).

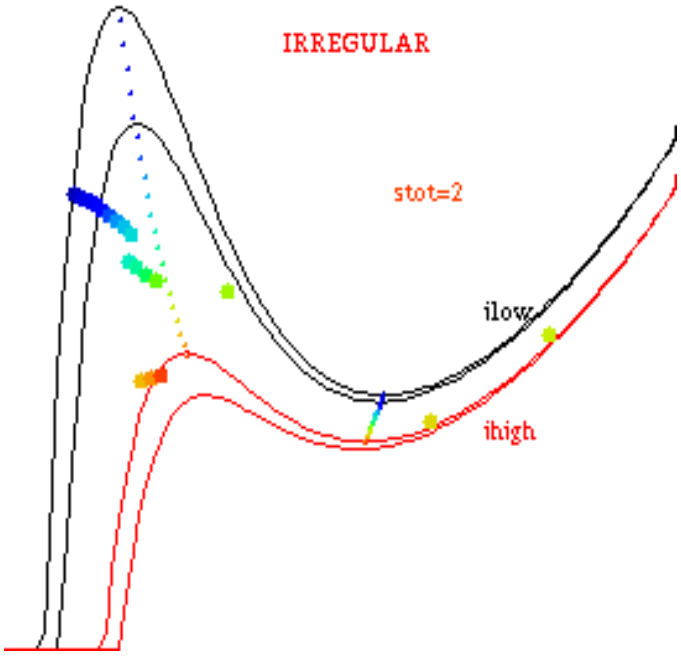

Figure 7. *Animation of a simulated irregular solution ($\bar{g}_{syn} = .0035$). In this still frame, note that cells with $I_{app} < I_{max}$ have jumped up first in this oscillation cycle. Since only two cells are active in the still frame, $s_{tot} = 2$.*

Now consider the silent phases, during which cells lie along the left branches of the appropriate cubics. We will assume that $G_L(h, I_{tot})$ is linear. More precisely, assume that there exist positive constants a, b, and c such that

$$h' = G_L(h, I_{tot}) = -ah - bI_{tot} + c. \tag{4.5}$$

This will be the case if $g(v, h)$ is given by (4.4), $h_\infty(v)$ is linear, $\tau_h(v)$ is constant, and each of the left branches is linear. Of course, none of these conditions are precisely satisfied. However, we demonstrate later that these assumptions lead to a very good approximation of the synchronized snake.

Remark 4.1. Recall that $h_{LK} = h_{LK}(I_{max})$, the h-value of the left knee of the v-nullcline for $I_{app} = I_{max}$. Since we assume that there is no fixed point on the left branch of the v-nullcline for $I_{app} = I_{max}$, we have

$$-ah_{LK} - bI_{max} + c > 0. \tag{4.6}$$

4.3. Jumping up. In section 5, we will consider synchronous snakes with the property that all of the cells jump up together, with respect to the slow time scale. In section 6, we consider snakes that jump up more gradually. The reason why simultaneous jump-up is possible is that, when one cell jumps up, the synaptic inputs to all of the other cells increase. This lowers the cubics associated with the other cells. If one of the other cells lies above the left

knee of its lowered cubic (i.e., above its effective left knee), then that cell will also jump up to the active phase, leading to the further lowering of the cubics. Since the jump-up takes place on the fast time scale and the Heaviside synaptic variables $s_\infty(v)$ respond instantaneously, it is possible for all of the cells to jump up together with respect to the slow time variable τ.

We now derive an expression for when the cells do jump up together as described above. Cells with $I_{app} = I_{max}$ jump up when they reach their left knee. Motivated by Remark 3.1, we assume that the cells that jump up do so in order of decreasing I_{app}. Fix $I \in [I_{min}, I_{max})$, and assume that each of the cells with $I < I_{app} < I_{max}$ jumps up at the same moment as $cell(I_{max})$. We wish to determine whether $cell(I)$ must also jump up at that moment, that is, whether it lies above the left knee of the appropriate cubic.

Let $(v(I), h(I))$ denote the position of $cell(I)$ in (v, h) phase space, where $v(I) = v_L(h(I), I)$, at the moment when the cells with $I_{app} > I$ jump up. From (2.4), it follows that the synaptic input to $cell(I)$ is

$$I^u_{syn}(I) \equiv (g_{syn}/Vol)(v_{syn} - v(I))\mu\{x : I_{app}(x) > I\}, \tag{4.7}$$

where μ is the usual Lebesgue measure and Vol is the same normalization factor given in (2.4). Essentially, $\mu\{x : I_{app}(x) > I\}$ gives the volume of the subset of D on which $I_{app}(x) > I$. We assume henceforth that $I^u_{syn}(I)$ is a continuously differentiable function of I on (I_{min}, I_{max}). Following the notation introduced in the preceding section, we find that $cell(I)$ will jump up if

$$h(I) > h_{LK}(I + I^u_{syn}(I)). \tag{4.8}$$

Hence, if this last condition is satisfied for all $I \in [I_{min}, I_{max}]$, then all of the cells will jump up together. In subsection 5.2, we demonstrate how this leads to an explicit condition on parameters and nonlinear functions in (2.2) for the existence of a snake of synchrony.

4.4. Jumping down. For the solutions under consideration in sections 5 and 6, all cells jump down at the same time with respect to τ, from right knees $h_{RK}(I)$ which depend on I. This is possible through a mechanism analogous to that described above for synchronous jump-up. Jump-down is initiated when $cell(I_d)$ reaches its right knee for some $I_d \in [I_{min}, I_{max}]$. Once this occurs, then, for each $I \neq I_d$, the loss of synaptic input to $cell(I)$ from the jumping down of other cells raises the effective right knee of $cell(I)$ sufficiently high that $h(I) < h_{RK}(I + I_{syn}(I))$ for the appropriate value of $I_{syn}(I)$, and $cell(I)$ jumps down. Since any $cell(I_d)$ may initiate the jump-down, writing an expression analogous to (4.7) for $I_{syn}(I)$ at jump-down becomes complicated (although, for special cases, we can derive a jump-down condition analogous to (4.8)). Instead, we simply assume that all cells jump down together. This assumption is based on numerics showing unified jump-down for all synchronous solutions. Moreover, while no cells have critical points on their right branches, all cells' right knees come close to $h_\infty(v)$ in the active phase for the parameter values in the appendix. Thus, based on (4.4), all cells become compressed toward their right knees in the active phase, promoting unified jump-down.

5. Linear snakes: Cells jump up and jump down together.

5.1. Snake formula. We assume throughout this section that all of the cells jump up and jump down together, with respect to the slow time scale. Although this condition may not hold, in general, we will demonstrate that, for strong coupling, it does lead to a very good approximation for the snake. We shall derive an explicit formula for the initial (jump-up) position $h(I) \equiv h(I,0)$ of a periodic snake of synchrony. It will follow that $h(I)$ must be linear in the case of synchronized jumps.

Suppose that the first cell to jump down is $cell(I_d)$ and this cell jumps down at the right knee, whose position we denote by h^d_{RK}. (Note that it is possible that $I_d \neq I_{max}$.) Then the time that cells spend in the active phase after they jump up is the time for $cell(I_d)$ to evolve from $h_d \equiv h(I_d)$ to h^d_{RK} under (4.3), namely, $T_A = \frac{1}{\rho}\ln(h_d/h^d_{RK})$. At this jump-down time, each cell has a position given by $h(I,T_A) = h(I)h^d_{RK}/h_d$.

We next consider when the cells are in the silent phase after they jump down. During this time, $I_{syn} = 0$. Hence each cell evolves according to (4.5) with $I_{tot} = I$ and initial position $h(I,T_A)$. It follows that, while in the silent phase,

$$h(I,\tau) = h(I)\frac{h^d_{RK}}{h_d}e^{a(T_A-\tau)} + \Lambda_I(1-e^{a(T_A-\tau)}), \tag{5.1}$$

where we set

$$\Lambda_I = (c-bI)/a, \tag{5.2}$$

which is the value of the critical point of (4.5) for $I_{syn} = 0$. One cycle is completed when $cell(I_{max})$ returns to its left knee, $h_{LK} \equiv h_{LK}(I_{max})$. If this is at time T, then, setting $T_S = T - T_A$, (5.1) yields

$$h(I,T) = h(I)\frac{h^d_{RK}}{h_d}e^{-aT_S} + \Lambda_I(1-e^{-aT_S}) \equiv M(h(I)). \tag{5.3}$$

Now a periodic snake of synchrony corresponds to a fixed point of the operator $M(h(I))$.

In particular, for $I = I_{max}$, setting $\Lambda_I = \Lambda_M \equiv \Lambda_{I_{max}}$ in (5.3) gives

$$h_{LK} \;=\; h_{LK}\frac{h^d_{RK}}{h_d}e^{-aT_S} + \Lambda_M(1-e^{-aT_S}).$$

Multiplying through by $h(I)/h_{LK}$ gives

$$h(I) = h(I)\frac{h^d_{RK}}{h_d}e^{-aT_S} + \frac{\Lambda_M h(I)}{h_{LK}}(1-e^{-aT_S}). \tag{5.4}$$

We now have expressions for $M(h(I))$, from the right-hand side of (5.3), and $h(I)$, from (5.4). The corresponding fixed point equation $M(h(I)) = h(I)$ has a unique solution, given by the analytic expression

$$h(I) = h_{LK}\left(\frac{\Lambda_I}{\Lambda_M}\right) \;=\; h_{LK}\left(\frac{c-bI}{c-bI_{max}}\right). \tag{5.5}$$

Note that the value of $h(I)$ given in (5.5) is attainable by the evolution of (4.5), since it lies below the critical point of (4.5) for each I. This holds since $h_{LK} < \Lambda_M$ by (4.6), while the critical point of the h-equation for fixed I is Λ_I. In Figure 8, the fixed point snake position at jump-up predicted by (5.5) is compared to the snake position at jump-up from numerical simulations of the pre-BötC network (2.2), with 20 cells, for $g_{syn}/20 = .012$, which leads to relatively simultaneous jumps (see Figures 2a and 3).

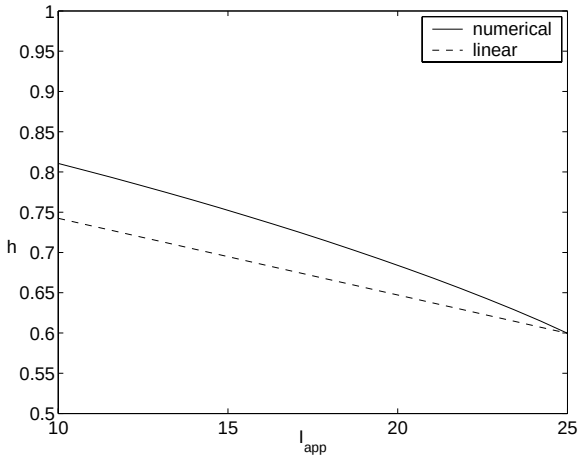

Figure 8. *Fixed point snake positions at jump-up. The dashed curve shows the estimate from formula* (5.5)*, and the solid curve shows the result from numerical simulations of* (2.2)*, with* 20 *cells, both for* $g_{syn}/20 = .012$.

Remark 5.1. Interestingly, formula (5.5) for the snake does not depend on any parameter associated with the active phase or the synaptic coupling between cells. Such parameters may affect whether or not cells all jump up together, but if this does happen, then (5.5) gives the position of the snake of synchrony at jump-up.

5.2. Jump-up condition. When deriving the snake formula, we assumed that all of the cells jumped up together. Here we use (4.8) to derive conditions on the parameters for when this must be the case. For simultaneous jump-up, the left-hand side of (4.8) is given by the snake formula given in (5.5). It remains, therefore, to estimate terms on the right-hand side of (4.8).

Choose λ_1 so that, if (v, h) lies in the silent phase (with $I_{syn} = 0$), then

$$v_{syn} - v > \lambda_1. \tag{5.6}$$

We assume that there exists $\lambda_2 > 0$ such that

$$\mu\{x : I_{app}(x) > I\} \geq \lambda_2(I_{max} - I) \tag{5.7}$$

for all $I \in [I_{min}, I_{max}]$. The existence of a strictly positive λ_2 such that (5.7) holds requires that the distribution of I values does not have an exponentially decaying "tail" near I_{max}. Such a tail would lead to a gradual jump-up, which is discussed in section 6.

Now let $I^u_{syn}(I)$ be as in (4.7), and set $\lambda_0 = \lambda_1\lambda_2$. It then follows from (4.7), (5.6), and (5.7) that

$$I^u_{syn}(I) \;>\; g_{syn}\lambda_0(I_{max} - I). \tag{5.8}$$

Finally, we assume that we can bound $h_{LK}(I)$ between two linear functions of I; that is, there exist positive constants m_1 and m_2 such that

$$m_1(I_{max} - I) < h_{LK}(I) - h_{LK} \;<\; m_2(I_{max} - I) \tag{5.9}$$

for all $I \in [I_{min}, I_{max}]$. (Recall that $h_{LK} \equiv h_{LK}(I_{max})$.) Together with (5.8), this implies that

$$h_{LK}(I + I^u_{syn}) < h_{LK} + m_2(I_{max} - I)(1 - g_{syn}\lambda_0). \tag{5.10}$$

A straightforward calculation, combining (4.8), (5.5), and (5.10), then demonstrates that (4.8) is satisfied if

$$g_{syn} > \frac{1}{\lambda_0}\left(1 - \frac{bh_{LK}}{am_2\Lambda_M}\right), \tag{5.11}$$

that is, if the synaptic coupling is sufficiently large.

When deriving the snake formula, we also assumed that $cell(I_{max})$ is the first to jump up. This will be the case if

$$h(I) \;=\; h_{LK}\frac{\Lambda_I}{\Lambda_M} \;<\; h_{LK}(I)$$

for all $I < I_{max}$. Using the left-hand side of (5.9), the definition of Λ_I from (5.2), and the notation $\Lambda_M := \Lambda_{I_{max}}$, we find that this holds if

$$m_1 > \frac{bh_{LK}}{a\Lambda_M}, \tag{5.12}$$

that is, if the curve of left knees is sufficiently steep.

Remark 5.2. In the simulations throughout this paper, the right-hand side of (5.12) is considerably smaller than m_1. This fits nicely with the fact that $cell(I_{max})$ jumps up first in all of the synchronized solutions that we observe.

Remark 5.3. In a similar manner to the above, we can derive conditions for which a cell hits its right knee first and for whether all cells jump down together when this occurs. Note, however, that the jump-down is in general observed to be well synchronized in our simulations, in full model simulations [3], and in experiments [12]. In the appendix, we also discuss how the parameters in (5.11) and (5.12) can be easily approximated from system (2.2), giving a means to predict whether system (2.2) can be expected to support synchronized oscillations with unified jump-up for particular parameter values. In the next section, we derive a more general formula for the snake in which we do not assume that all of the cells jump up at the same time on the fast time scale.

5.3. Stability of the fixed point snake of synchrony. In this subsection, we consider stability of the fixed point (5.5) representing the snake of synchrony, from two perspectives. The map given in (5.3) is nonlocal since the term $h(I_d)$ appears explicitly in it for all I, and this complicates stability analysis. We start by considering the class of linear snakes. That is, we restrict ourselves to snakes that satisfy initial conditions of the form

$$h(I,0) \;=\; h(I) \;=\; h_{LK} + \alpha(I_{max} - I) \tag{5.13}$$

at jump-up for an arbitrary parameter α. It is easy to check that a solution of (4.3) and (4.5), with simultaneous jumps between phases, remains linear if it satisfies (5.13) at jump-up. We derive a map on slopes α defined for linear snakes, with a fixed point corresponding to (5.5), and use this to prove that the snake of synchrony is stable within the class of linear snakes. After this, we derive a sufficient condition for this snake of synchrony to be nonlinearly stable, without restriction of solution class.

Because solutions with initial conditions that are linear functions of I remain linear for all time, the initial condition (5.13) evolves after one cycle into another linear function of I, possibly with a different slope. We write this as

$$h(I,T) \;=\; h_{LK} + \pi(\alpha)(I_{max} - I).$$

Here T is the cycle duration. This naturally gives rise to a real map $\alpha \to \pi(\alpha)$. We wish to derive a formula for this map, find the fixed point corresponding to (5.5), and determine its stability.

Recall that $h' = -\rho h$ in the active phase. Consistent with our earlier notation, we fix I_d such that $cell(I_d)$ jumps down first. As previously, let $h_d = h(I_d, 0)$, let h^d_{RK} denote the value of h at the right knee for $I = I_d$, and recall that T_A denotes the time spent by all cells in the active phase. Then (4.5) yields

$$h(I,T_A) = (h_{LK} + \alpha(I_{max} - I))\, e^{-\rho T_A}, \tag{5.14}$$

where

$$e^{-\rho T_A} = \frac{h^d_{RK}}{h_d}. \tag{5.15}$$

As previously, in the silent phase, $h' = -ah - bI + c$, and $\Lambda_I = (c - bI)/a$. Solving this silent phase equation with initial condition (5.14) yields that, for $T_A < \tau < T$,

$$h(I,\tau) = h(I,T_A)e^{a(T_A-\tau)} + \Lambda_I(1 - e^{a(T_A-\tau)})$$

or, letting $T_S = T - T_A$,

$$h(I,T) = (h_{LK} + \alpha(I_{max} - I))\, e^{-\rho T_A}e^{-aT_S} + \Lambda_I(1 - e^{-aT_S}). \tag{5.16}$$

Note that $h(I_{max}, T) = h_{LK}$. Hence, for $\Lambda_M := \Lambda_{I_{max}}$, as previously,

$$h_{LK} = h_{LK}e^{-\rho T_A}e^{-aT_S} + \Lambda_M(1 - e^{-aT_S}). \tag{5.17}$$

We use this last equation along with (5.16) to conclude that

$$h(I,T) \;=\; h_{LK} + \alpha(I_{max} - I)e^{-\rho T_A}e^{-aT_S} + (\Lambda_I - \Lambda_M)(1 - e^{-aT_S})$$

or

$$h(I,T) \;=\; h_{LK} + (I_{max} - I)\left(\alpha e^{-\rho T_A}e^{-aT_S} + \frac{b}{a}(1 - e^{-aT_S})\right).$$

It follows that

$$\pi(\alpha) = \alpha e^{-\rho T_A}e^{-aT_S} + \frac{b}{a}(1 - e^{-aT_S}). \tag{5.18}$$

To rewrite (5.18), note that, from (5.17),

$$e^{-\rho T_A}e^{-aT_S} \;=\; 1 - \frac{\Lambda_M}{h_{LK}}(1 - e^{-aT_S}), \tag{5.19}$$

which implies, after some rearrangement, that

$$\pi(\alpha) = \alpha + \left(\frac{b}{a} - \alpha\frac{\Lambda_M}{h_{LK}}\right)(1 - e^{-aT_S}). \tag{5.20}$$

Finally, solving $\pi(\alpha_0) = \alpha_0$ yields an expression for the fixed point α_0, namely,

$$\frac{b}{a} - \alpha_0\frac{\Lambda_M}{h_{LK}} = 0 \quad \text{or} \quad \alpha_0 = \frac{b}{a}\frac{h_{LK}}{\Lambda_M}. \tag{5.21}$$

Remark 5.4. Note that the slope specified in (5.21) is exactly that of the fixed point snake (5.5), and so our two calculations are consistent. However, the calculation here is not as general as the earlier one in subsection 5.1, which, in theory, allowed for the possibility of nonlinear fixed points.

Next we consider the stability of the fixed point. We differentiate (5.20) to find that

$$\pi'(\alpha) \;=\; 1 - \frac{\Lambda_M}{h_{LK}}(1 - e^{-aT_S}) + \left(\frac{b}{a} - \alpha\frac{\Lambda_M}{h_{LK}}\right)ae^{-aT_S}\frac{dT_S}{d\alpha}. \tag{5.22}$$

The last term is zero for $\alpha = \alpha_0$ because of (5.21). Hence

$$\pi'(\alpha_0) = 1 - \frac{\Lambda_M}{h_{LK}}(1 - e^{-aT_S}). \tag{5.23}$$

In order to make sense of this, we substitute (5.15) into (5.17) to find that

$$h_{LK} \;=\; h_* e^{-aT_S} + \Lambda_M(1 - e^{-aT_S}),$$

where

$$h_* \equiv h_{LK}\frac{h_{RK}^d}{h_d}. \tag{5.24}$$

Hence

$$e^{-aT_S} = \frac{\Lambda_M - h_{LK}}{\Lambda_M - h_*}. \tag{5.25}$$

Apply this in (5.23), and use (5.24) to find

$$\begin{aligned} \pi'(\alpha_0) &= 1 - \frac{\Lambda_M}{h_{LK}} \frac{(h_{LK} - h_*)}{(\Lambda_M - h_*)} \\ &= 1 - \Lambda_M \left(\frac{1 - \frac{h^d_{RK}}{h_d}}{\Lambda_M - h_{LK} \frac{h^d_{RK}}{h_d}} \right). \end{aligned} \tag{5.26}$$

The last term in (5.26) is positive because $h^d_{RK} < h_d$ and $h_{LK} < \Lambda_M$ from (4.6). Therefore, we wish to prove that it is less than 2. We will, in fact, show that this last term is less than 1, and, therefore, $0 < \pi'(\alpha_0) < 1$. This follows if

$$\Lambda_M - \Lambda_M \frac{h^d_{RK}}{h_d} < \Lambda_M - h_{LK} \frac{h^d_{RK}}{h_d},$$

which is true because $h_{LK} < \Lambda_M$. Thus the snake of synchrony is stable within the class of linear snakes.

Remark 5.5. When $I_d = I_{max}$, the map in (5.3) no longer depends on an unknown $h_d \equiv h(I_d, 0)$ since, by construction, $h(I_{max}, 0) = h_{LK}$. Thus (5.3) becomes linear in h and can be differentiated directly with respect to h. The derivative of the map is exactly the expression given in (5.26). Thus, for $I_d = I_{max}$, the fixed point snake of synchrony is always stable. However, this calculation is not possible for $I_d \neq I_{max}$.

To consider stability without restriction to the class of linear snakes or to $I_d = I_{max}$, we consider perturbations sufficiently small such that they do not change which cells jump down first (i.e., the value of I_d). Clearly such perturbations exist; as an example, recall from section 3 that there is a range of g_{syn} values that gives a snake of synchrony for which cells with $I = I_{max}$ jump down first. For such a snake, a perturbation that retards the other cells slightly and is sufficiently small to preserve synchrony conserves I_d.

Let $h(I)$ denote the snake of synchrony, and let $p(I) = h(I) + \epsilon(I)$ denote a perturbation of $h(I)$ at jump-up. We will measure distance under the supremum norm $||f(I)|| = \sup\{|f(I)| : I \in [I_{min}, I_{max}]\}$. We will derive a condition under which, for $M(h(I))$ defined in (5.3), we have $||M(p) - M(h)|| \leq L||p - h||$ for a constant $0 < L < 1$. Equation (5.3) gives

$$||M(p) - M(h)|| = ||h(I)h^d_{RK} e^{-aT_S}/h_d - p(I)h^d_{RK} e^{-a\tilde{T}_S}/p_d - \Lambda_I(e^{-aT_S} - e^{-a\tilde{T}_S})||,$$

where e^{-aT_S} is given by (5.25), $p_d = p(I_d)$, and $\tilde{T}_S$ is the value of T_S obtained by substituting p_d for h_d in $h_* = h_{LK}h^d_{RK}/h_d$. Some algebraic manipulation yields, for $\epsilon_d = \epsilon(I_d)$,

$$||M(p) - M(h)|| \leq (\Lambda_M - h_{LK}) \left|\left| \frac{p(I)h^d_{RK} - \Lambda_I(h_d + \epsilon_d)}{K - \Lambda_M \epsilon_d} - \frac{h(I)h^d_{RK} - \Lambda_I h_d}{K} \right|\right|, \tag{5.27}$$

where $K = h_{LK}h^d_{RK} - \Lambda_M h_d$ is independent of I. Note that $K < 0$ since $\Lambda_M > h_{LK}$ and $h_d > h^d_{RK}$.

Expand the right-hand side of (5.27) in ϵ_d, and note that $|\epsilon_d| \le ||\epsilon||$ to obtain

$$||M(p) - M(h)|| \le \left(\frac{(\Lambda_M - h_{LK})||\epsilon||}{|K|}\right)\left(h^d_{RK} + \left|\left|\frac{\Lambda_M(p\,h^d_{RK} - \Lambda_I h_d) - \Lambda_I K}{K}\right|\right|\right) + O(\epsilon^2).$$

For ϵ sufficiently small, the higher order terms can be neglected, and application of the definition of K yields

$$||M(p) - M(h)|| \le \left(\frac{(\Lambda_M - h_{LK})h^d_{RK}||\epsilon||}{|K|}\right)\left(1 + \left|\left|\frac{p\,\Lambda_M - \Lambda_I h_{LK}}{K}\right|\right|\right). \tag{5.28}$$

Let S denote $\sup_I(p(I)\Lambda_M - \Lambda_I h_{LK})$, the difference of two positive terms. It remains to estimate S. Suppose that $S > 0$. Then the two relations $p(I) \le \Lambda_I$ and $\Lambda_{I_{min}} = \max_I(\Lambda_I)$, which follow from (5.2), and $\Lambda_M > h_{LK}$ from (4.6) give $S \le \Lambda_{I_{min}}(\Lambda_M - h_{LK})$. Suppose instead that $S < 0$. For concreteness, we assume that $p(I) \ge h_{LK}$ for all I, which holds for sufficiently small perturbations. Then $|S| \le h_{LK}(\Lambda_{I_{min}} - \Lambda_M)$. Thus $|S| \le \max\{\Lambda_{I_{min}}(\Lambda_M - h_{LK}), h_{LK}(\Lambda_{I_{min}} - \Lambda_M)\} \equiv \bar{S}$.

For this $\bar{S}$, (5.28) implies that, if the condition

$$\frac{(\Lambda_M - h_{LK})h^d_{RK}}{|K|}\left(1 + \frac{\bar{S}}{|K|}\right) < 1$$

holds, then the snake of synchrony is stable with respect to sufficiently small perturbations. This condition holds for a variety of numerical examples that we have considered. Note that it certainly holds when h_{LK} lies near the fixed point Λ_M, since K is bounded away from zero as $h_{LK} \to \Lambda_M$, as long as the h-values on the curves of left and right knees remain separate.

6. Nonlinear snakes. In the previous section, we assumed that the cells jump up and jump down together on the slow time scale. This will be the case if g_{syn}, the synaptic strength, is sufficiently strong. Numerical simulations demonstrate that, for smaller g_{syn}, the jump-up and jump-down processes are more gradual, as shown in Figures 2b and 4. Each cell jumps up or down when it reaches the left or right knee of its effective cubic. In the analysis here, we allow the cells to jump up at different times on the slow time scale, but we still assume that the cells jump down at the same time. We shall derive a nonlinear boundary value problem for the periodic snake of synchrony. An analogous derivation leads to a similar formula if there is a gradual jump-down.

We denote the position of the snake as $h(I, \tau)$. It will be convenient to choose the translation now so that $\tau = 0$ corresponds to the moment when all of the cells jump down. In addition to assuming that all of the cells jump down together, we will further assume that the jump-down process begins when $cell(I_{max})$ reaches its right knee at $h = h_{RK}$, consistent with numerical simulations of the gradual jump-up case (section 3). Let $h_0(I) \equiv h(I, 0)$ denote the corresponding initial position of the snake.

We assume that the first cells to jump up are $cell(I_{max})$. Moreover, the cells jump up in order of decreasing I. As before, let T_S be the time for $cell(I_{max})$ to evolve under (4.5) from h_{RK} up to h_{LK}. We let $h_\mu(I) \equiv h(I, T_S)$ denote the position of the snake when $cell(I_{max})$ jumps up. We then let $\Delta(I)$ denote the delay in the jump-up of $cell(I)$ relative to $cell(I_{max})$.

That is, $\Delta(I_{max}) = 0$, and $cell(I)$ jumps up at $\tau = T_S + \Delta(I)$. We shall derive three equations for the three unknown functions $h_0(I), h_\mu(I)$, and $\Delta(I)$.

First, we consider the cells while all are in the silent phase. The cells then evolve according to (4.5) from their initial position $h_0(I)$ to $h_\mu(I)$ at time T_S. Solving (4.5), we find that

$$h_0(I) = (h_\mu(I) - \Lambda_I)e^{aT_S} + \Lambda_I.$$

Substitution of the formula for e^{aT_S} (see (5.25)) yields the first equation,

$$h_0(I) = (h_\mu(I) - \Lambda_I)\left(\frac{h_{RK} - \Lambda_M}{h_{LK} - \Lambda_M}\right) + \Lambda_I. \tag{6.1}$$

We next follow the cells forward after they jump up. Denote the position of the left knee at which $cell(I)$ jumps up as

$$(v_{LK}^{eff}, h_{LK}^{eff})(I) \equiv (v_{LK}, h_{LK})(I + I_{syn}^u(I)).$$

Recall that this is found by solving $f + I + I_{syn}^u(I) = 0$, where $I_{syn}^u(I)$ is given by (4.7) and implicitly depends on v, for $v = v_L(h, I)$, and then solving $\partial(f + I_{syn}^u(I))/\partial v = 0$ for $(v_{LK}^{eff}(I), h_{LK}^{eff}(I))$ on this curve. Since cells jump up at different times but jump down together, they spend different amounts of time in the active phase. We again use $h' = -\rho h$ for evolution in the active phase, as indicated in (4.3). We saw earlier that, according to this equation, $cell(I_{max})$ spends time $T_A = (1/\rho)\ln(h_{LK}/h_{RK})$ in the active phase. Each cell with $I < I_{max}$ spends time $T_A - \Delta(I)$ in the active phase, starting from initial condition $h_{LK}^{eff}(I)$ and ending at its jump-down position $h_0(I)$. Using this to solve (4.3) yields the second equation,

$$h_0(I) = h_{LK}^{eff}(I)\left(\frac{h_{RK}}{h_{LK}}\right)e^{\rho\Delta(I)}. \tag{6.2}$$

To obtain the third equation, we follow each $cell(I)$ in the silent phase from $\tau = T_S$ until $cell(I)$ jumps up. First, we need to introduce some notation. Let $I_{syn}(\tau)$ denote the synaptic input at time τ. We earlier let $I_{syn}^u(I)$ be the synaptic input when $cell(I)$ jumps up. Since $cell(I)$ jumps up when $\tau = T_S + \Delta(I)$, it follows that $I_{syn}^u(I) = I_{syn}(T_S + \Delta(I))$, where $I_{syn}^u(I)$ is given by (4.7) with $v(I) = v_{LK}^{eff}(I)$.

Now each $cell(I)$ satisfies (4.5) with $I_{tot} = I + I_{syn}(\tau)$. Moreover, $h(I, T_S) = h_\mu(I)$, and $cell(I)$ jumps up at $h_{LK}^{eff}(I)$, the left knee of its effective cubic, when $\tau = T_S + \Delta(I)$. Solving (4.5) with these boundary conditions, we find that

$$h_{LK}^{eff}(I) = (h_\mu(I) - \Lambda_I)e^{-a\Delta(I)} + \Lambda_I - be^{-aT_S}e^{-a\Delta(I)}\int_{T_S}^{T_S+\Delta(I)} I_{syn}(\tau)e^{a\tau}\,d\tau. \tag{6.3}$$

Equations (6.1), (6.2), and (6.3) constitute a system of three equations in the three unknowns $h_0(I), h_\mu(I)$, and $\Delta(I)$. From (6.2), $\Delta(I)$ can be expressed as a function of $h_0(I)$. Equations (6.1) and (6.3) are easily converted into formulas for $h_\mu(I)$. Equating these formulas gives, after minor rearrangement,

$$h_0(I) = \Lambda_I + \Gamma\left((h_{LK}^{eff}(I) - \Lambda_I)e^{a\Delta(I)} + be^{-aT_S}\int_{T_S}^{T_S+\Delta(I)} I_{syn}(\tau)e^{a\tau}\,d\tau\right), \tag{6.4}$$

where $\Delta(I)$ is now a function of $h_0(I)$ and where $\Gamma = (h_{RK} - \Lambda_M)/(h_{LK} - \Lambda_M)$.

To solve (6.4) for $h_0(I)$, we first differentiate with respect to I to obtain

$$\begin{aligned} h_0'(I) = \Lambda_I' &+ \Gamma((h_{LK}^{eff})'(I) - \Lambda_I')e^{a\Delta(I)} \\ &+ a\Gamma(h_{LK}^{eff}(I) - \Lambda_I)\Delta'(I)e^{a\Delta(I)} \\ &+ b\Gamma I_{syn}(T_S + \Delta(I))\Delta'(I)e^{a\Delta(I)}. \end{aligned} \tag{6.5}$$

Recall that $I_{syn}(T_S + \Delta(I)) = I_{syn}^u(I)$, where $I_{syn}^u(I)$ is given by (4.7) with $v(I) = v_{LK}^{eff}(I)$. Moreover, we can use (6.2) to solve for $\Delta(I)$ and $\Delta'(I)$. In fact, if we let

$$\Phi(I) \equiv e^{\rho\Delta(I)} = \left(\frac{h_{LK}}{h_{RK}}\right)\frac{h_0(I)}{h_{LK}^{eff}(I)}, \tag{6.6}$$

then a straightforward calculation starting from (6.2) demonstrates that

$$\Delta'(I)e^{a\Delta(I)} = \frac{1}{\rho}\Phi'(I)\Phi^{(a-\rho)/\rho}.$$

Substituting this into (6.5), we find that

$$\begin{aligned} h_0'(I) = \Lambda_I' &+ \Gamma((h_{LK}^{eff})'(I) - \Lambda_I')\Phi^{a/\rho}(I) \\ &+ \frac{a}{\rho}\Gamma(h_{LK}^{eff}(I) - \Lambda_I)\Phi'(I)\Phi^{(a-\rho)/\rho}(I) \\ &+ \frac{b}{\rho}\Gamma I_{syn}^u(I)\Phi'(I)\Phi^{(a-\rho)/\rho}. \end{aligned} \tag{6.7}$$

We can use (6.6) to write $\Phi(I)$ and $\Phi'(I)$ in terms of $h_0(I)$ and $h_0'(I)$. Equation (6.7) then gives an ordinary differential equation for $h_0(I)$, the initial (jump-down) position of the periodic snake. Note that the solution must satisfy the boundary condition $h(I_{max}) = h_{RK}$. Solving the resulting boundary value problem numerically with XPPAUT gives an estimate of $h_0(I)$. We can compute $h_\mu(I)$, the position of the snake when $cell(I_{max})$ is ready to jump up, directly from this, using (6.1). Figure 9 compares the resulting $h_\mu(I)$ (dotted curve) with the snake position from a full numerical simulation of the pre-BötC model network (solid curve) and with the linear snake formula (5.5), all for $g_{syn}/20 = .009$, which corresponds to gradual jump-up (see Figures 2b and 4). For the nonlinear and linear curves, parameters were estimated from the pre-BötC model without simulations, using the methods discussed below in the appendix. Because it takes gradual jump-up into account, the nonlinear result gives a better approximation of the snake position than does the linear formula, in the gradual jump-up case.

Remark 6.1. We can perform analogous calculations to derive an ordinary differential equation boundary value problem for the jump-up snake of synchrony $h_\mu(I)$ in the case of gradual jump-down and simultaneous jump-up. The resulting ordinary differential equation analogous to (6.7) is simpler because there is one fewer unknown: $h_\mu(I)$ and $h_{LK}^{eff}(I)$ collapse to the same curve. The ordinary differential equation in that case is explicitly nonlocal, however, in that Γ depends on $h_\mu(I_{min})$, such that the right-hand side depends on I_{min} for all I; nonetheless, it can be solved numerically with XPPAUT without a problem.

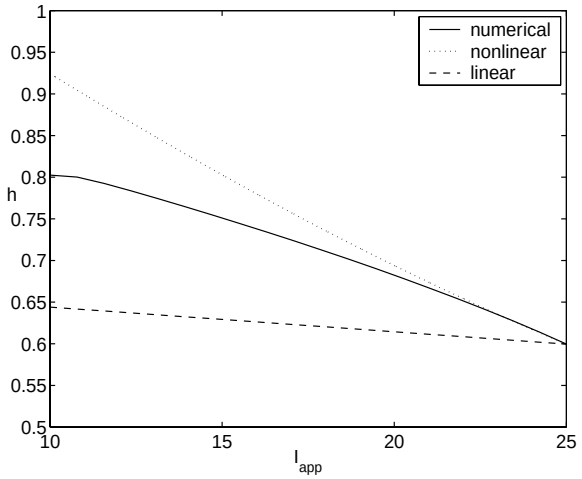

Figure 9. *Snake of synchrony at the moment when leading cells jump up. The plot shows curves for* $g_{syn}/20 = .009$*, corresponding to gradual jump-up.*

7. Loss of synchrony.

7.1. Break-up conditions. The analysis in section 5 shows that there is only one possible fixed point snake for the case in which all cells jump up and jump down together. Suppose that condition (4.8) fails for some I values, so that this solution does not exist and not all cells jump up together. In section 6, we consider another form of synchronized oscillation in which cells jump up more gradually until all are in the active phase. In this subsection, we find a sufficient condition for break-up of the synchronized solution by computing a condition under which not all cells reach jump-up before the leading cells, with $I = I_{max}$, jump down from the active phase. This computation can also lead to an estimate for the I value at which the snake will break.

First, we assume that cells with $I = I_{max}$ jump down first on every oscillation cycle. For fixed intrinsic cellular parameters, this corresponds to taking g_{syn} small enough. This is quite natural for the consideration of loss of synchrony since a large synaptic coupling strength promotes synchronization.

We start at time $\tau = 0$ with cells at $h(I, 0)$, a position for which cells with $I = I_{max}$ are about to jump up. To derive a break-up condition, we now compute a condition under which not all cells can evolve in the silent phase from $h(I, 0)$ to their effective knees before cells with $I = I_{max}$ jump down. Since we aim for a sufficient condition for break-up, we assume the fastest possible silent phase evolution corresponding to $I_{syn} = 0$. Specifically, we solve

$$\begin{aligned} h' &= -ah - bI + c, \\ h(0) &= h(I, 0) \end{aligned} \tag{7.1}$$

for $h(I, \tau)$, up until time $T_A = \frac{1}{\rho} \ln \frac{h_{LK}}{h_{RK}}$, when the active cells jump down; this easily can be done analytically. The break-up condition is that, for some $I_b \in (I_{min}, I_{max})$,

$$h(I_b, T_A) = h_{LK}(I_b + I^u_{syn}(I_b)), \tag{7.2}$$

where $h_{LK}(I_b + I^u_{syn}(I_b))$ denotes the effective knee for $I = I_b$. If we restrict ourselves to snake configurations for which cells jump up in order of decreasing I, then all cells with $I < I_b$ fail to jump up at all during the oscillation; see Figure 10.

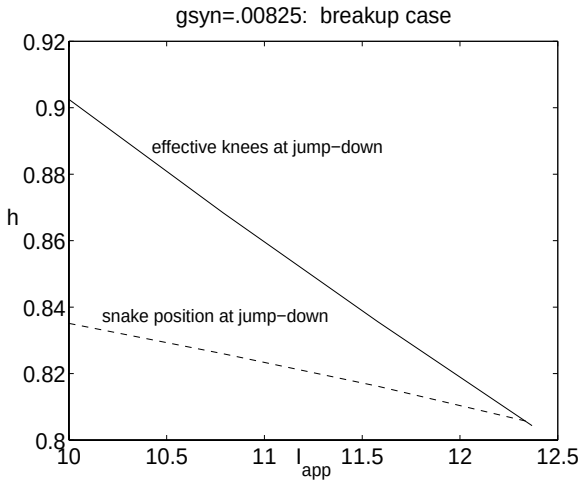

Figure 10. *Numerical illustration of the break-up of a snake. The network was simulated with* $g_{syn}/20 = .00825$*, as in Figures* 5a *and* 6 *in section* 3*. The cells gradually jump up, until cell*$(I_{max} = 25)$ *jump down, after which no other cells jump up. The plot shows the silent phase positions of the cells that fail to jump up, at the moment when cell*(I_{max}) *jumps down, as a function of* I_{app}*. Note that the nonjumping cells lie below their numerically computed effective left knees, with cell position intersecting the effective knee curve at the break point of the snake.*

Equation (7.2) can allow us to solve for the I_b at which a break occurs (if such an I value exists). If we wish just to check whether or not a break occurs, again assuming jump-up in order of decreasing I, we simply need to compare $h(I_{min}, T_A)$ to $h_{LK}(I_{min} + I^u_{syn}(I_{min}))$. That is, break-up occurs for some $I \geq I_{min}$ if

$$h(I_{min}, T_A) < h_{LK}(I_{min} + I^u_{syn}(I_{min})). \tag{7.3}$$

As an example, we can compute $h(I_{min}, T_A)$ for the fixed point snake configuration derived earlier by solving (7.1), with $h(0) = h_{LK}(c - bI_{min})/(c - bI_{max})$ from (5.5), for time T_A, which yields

$$h(I_{min}, T_A) = \Lambda_{I_{min}} \left[1 + \left(\frac{h_{RK}}{h_{LK}} \right)^{a/\rho} \left(\frac{h_{LK}}{\Lambda_M} - 1 \right) \right] < \Lambda_{I_{min}}.$$

Since I_{min} is the minimum value of I_{app}, for most I_{app} distributions, (4.7) gives $I^u_{syn}(I_{min}) \approx g_{syn}(v_{syn} - v(I_{min}))$. From the appendix, we thus have $I^u_{syn}(I_{min}) \approx g_{syn}(v_{syn} - (I_{min}/g_L + v_L))$. Hence all of the parameters needed to check inequality (7.3) can be estimated, as discussed in the appendix.

8. Discussion.

We have considered a reduced model for a network of conditional pacemaker cells in the pre-BötC of the brain stem. In this model, each cell is represented by a pair of ordinary differential equations, with excitatory synaptic coupling between the cells. The network is heterogeneous in that cells take values of a parameter I_{app} from a distribution.

Heterogeneities in I_{app} represent different levels of applied current (including sustained excitatory inputs from other brain regions) and different leak reversal potentials among different cells.

We analyze this system in the continuum limit for which the coupling terms become integrals. We consider oscillatory solutions for which each cell undergoes sustained silent and active phases, with occasional rapid jumps between the two, but we do not consider individual spikes within the active phases. This leads to a natural further reduction of the model, such that each cell is governed by the scalar equations (4.5) and (4.3) for the evolution of the slow variable h in the silent and active phases, respectively.

With these simplifications, we treat two forms of periodic, synchronized solutions, or "snakes": solutions for which all cells jump up and down simultaneously (on a slow time scale), and solutions which feature gradual jumps. Indeed, a key point here is that heterogeneous networks of synaptically coupled oscillating cells can support periodic, synchronized solutions with a continuum of phase shifts between jump times of different cells. This allows for a richer range of dynamics than has been observed for a homogeneous network of relaxation oscillators [16] or a network of oscillators with dynamics and coupling based on phases [22, 15, 9, 1].

We provide natural geometric conditions for the case of simultaneous jumps to occur. When these hold, we prove the existence of a unique periodic snake, characterized by a simple formula. This formula does not depend on any of the parameters associated with the active phase or synaptic coupling; however, these do appear in the conditions for simultaneous jumping. We also show that this snake is linearly stable to certain small perturbations, and we provide a general nonlinear stability condition. We note that our analysis of simultaneous jump solutions generalizes immediately to any finite population of oscillators; the continuum limit is not required here. In particular, with a finite number of oscillators, the effective left knee for cells with fixed I is determined by computing the synaptic input that results when all cells with larger I jump up, now based on the discrete synaptic current (2.3) rather than the continuum current (2.4).

When the synaptic coupling strength in the network is weakened, the conditions for simultaneous jumping may fail. In the case of gradual jumps up from the silent phase to the active phase, we derive a single nonlinear ordinary differential equation boundary value problem for the position of the periodic snake in phase space at a certain stage in its oscillatory cycle. This generalizes naturally to gradual jumps down or gradual jumps in both directions.

For our analysis, although we require that each cell have a cubic v-nullcline when uncoupled, we do not require that all cells be intrinsic oscillators when uncoupled, which is consistent with experimental observations. Thus our analysis illustrates how heterogeneities in a network can lead to robust, stable oscillations by allowing intrinsically active cells to recruit silent cells via synaptic coupling. We emphasize that such solutions can be periodic and synchronized in the sense that all cells begin and end their active phases together in time despite significant heterogeneities. In the synchronized solutions that we consider, cells may jump up to the active phase by reaching a curve of knees, or saddle-node bifurcation points of a fast subsystem. Alternately, synaptic coupling may cause cells to suddenly lie above this curve and therefore to jump up immediately. Based on other studies of bursting (see [16]) and our own simulations, we expect that the inclusion of spiking currents will not qualitatively affect the relevant bifurcations and the corresponding knees for jump-up. Since the dynamics

of the jump-up appears to be the key determinant of how well the network synchronizes, we therefore posit our results as an explanation for how heterogeneities enhance the tendency for a network of bursting cells, such as the pre-BötC, to fire synchronized bursts.

For all of our analysis, we assume all-to-all coupling. In the all-to-all case, all cells receive the same amount of coupling, depending only on the proportion of cells in the population that are active. Simulations in [3] yielded qualitatively similar network behavior for full and sparse network connectivities. Other coupling architectures would complicate analysis, however, especially if nonlocal or random connections were included.

In addition to analysis, we present numerical simulations to illustrate our results. These include comparisons of snake positions from full network simulations, performed with a discrete population of 20 cells with a uniform distribution of I_{app}, to snake positions computed from our analysis. To generate the latter, we estimate a variety of parameters, in particular those appearing in (5.5), (6.6), and (6.7), directly from the network equations (2.2); this can be done quite easily, as discussed in the appendix. Perhaps the most useful numerical results presented are animations of full network simulations. These show cells' positions in phase space, along with relevant nullclines and curves of knees. The nullclines and knees move as synaptic coupling strength changes over the course of a simulation. This allows for very clear visualization of the jumping behavior of individual cells, highlighting its dependence on the heterogeneity parameter I_{app}. We anticipate that such animations will be useful for a wide variety of studies of systems of coupled oscillators.

As g_{syn} drops still farther from the gradual jumping case, synchrony may in fact be lost. We provide a sufficient geometric condition for synchrony to fail. When synchrony breaks down, interesting periodic or possibly chaotic solutions can arise; we have illustrated two of these numerically. In general, the population's activity pattern for fixed parameter values can be classified according to the population of cells that become active on each cycle. Following [1], we can distinguish between locking, in which all cells fire on each cycle, partial locking, in which all cells fire but some cells skip some cycles, partial death, in which some cells never fire, and death, in which no cells fire. In simulations, we find that, for uniform distributions of I_{app}, with fixed mean I_{app} but different distribution widths γ, certain general trends emerge. For fixed γ, as coupling strength g_{syn} increases, the tendency to lock increases. Correspondingly, the population undergoes transitions from partial death, to partial locking, to locking as g_{syn} increases. Larger g_{syn} is required for more unified activity with larger γ, corresponding to a broader distribution of I_{app}; thus the partial locking and partial death regions form positively sloped bands in (γ, g_{syn}) parameter space. As the system switches from partial death to partial locking, there is a decrease in the variance across cells, in terms of the proportion of cycles during which each cell is active, until finally no variance remains in the locked state. Nonuniform distributions of I_{app} are expected to yield qualitatively similar trends. Work to analyze asynchronous solutions is in progress.

The heterogeneities that we consider are restricted to the parameter I_{app}, which includes heterogeneities both in the leak current reversal potential v_L and in applied current. Earlier studies have suggested that the biological effects of heterogeneities in pre-BötC cells are captured by heterogeneities in I_{app} (defined to include v_L) and g_{Na} [2]. The former, which we have considered here, is perhaps more relevant to ongoing biological experimentation because the leak reversal potential can be controlled by manipulation of potassium ion concentration

in an experimental preparation [6, 7]. Nonetheless, the role of g_{Na} should be explored to gain a full understanding of pre-BötC behavior.

9. Appendix.

9.1. Model equations and parameter values.

In system (2.2), we have, for $x = m$ or h,

$$x_\infty(v) = 1/(1+\exp((v-\theta_x)/\sigma_x)) \quad \text{and} \quad \tau_h(v) = (\epsilon \cosh((v-\theta_h)/2\sigma_h))^{-1}.$$

When we simulate a discrete population of 20 cells, we take

$$I_{syn} = g_{syn}\left(\sum_{k=1}^{20} s_\infty(v_k)\right)(v_{syn} - v_j)$$

as the synaptic input to cell j (that is, g_{syn} is already scaled to take into account the population size, since we always use 20 cells); $v_{syn} > v_j$ for solutions v_j, for the parameter values used. We further take $s_\infty(v_k) = 1/(1+\exp((v_k-\theta_s)/\sigma_s))$.

Parameter values used in simulations are given in Table 1, with units omitted. The parameter g_{syn} is varied, as indicated in figure captions. We use 20 cells, and I ranges over 20 equally spaced values, starting with $I_{min} = 10$ and ending with $I_{max} = 25$. For these parameters, there is a transition from excitable to oscillatory at around $I = 12.5$, such that cells with $I < 12.5$ will converge to a rest point in the silent phase without synaptic input. Thus we have cells that intrinsically are silent and cells that intrinsically are oscillators represented in our simulations. Note that the value of C_m used here is smaller than that in [2, 3, 6]. This accentuates the relaxation aspect of the oscillations that we study.

Table 1

Basic set of parameter values for the reduced pre-BötC cell model.

Parameter	Value	Parameter	Value	Parameter	Value	Parameter	Value
g_{Na}	2.8	v_{Na}	50	θ_m	-37	σ_m	-6
				θ_h	-44	σ_h	6
g_L	2.8	v_L	-65				
		v_{syn}	0	θ_s	-43	σ_s	-0.1
C_m	0.21	ϵ	0.01				

9.2. Estimation of parameters for numerics.

To generate the snake position numerically, given (5.5), we need only to estimate the parameters h_{LK}, b, c. Let the point (v_{LK}, h_{LK}) denote the solution to the two equations $F(v,h) = 0$ and $F_v(v,h) = 0$, where $F(v,h)$ denotes the right-hand side of the v-equation in (2.2) for $I_{syn} = 0$ and $I_{app} = I_{max}$. These easily can be solved numerically. In particular, they can be solved dynamically through the following procedure, which was used to generate the knee positions for all I_{app} in our animations. First, note that $F(v,h) = 0$ can be solved algebraically for $h(v)$. Next, let $y' = \phi F_v(v, h(v))$ for a large constant ϕ designed to speed up the convergence of y to v_{LK}. Once y converges sufficiently close to a steady value, then we denote this by v_{LK}, and we read out $h_{LK} = h(v_{LK})$.

For fixed I_{app}, we can estimate the value of v for a solution of (2.2) in the silent phase when $I_{syn} = 0$. To do this, we note that $m_\infty(v) \approx 0$ in the silent phase, such that $C_m v' \approx$

$-g_L(v - v_L) + I_{app}$. But the silent phase is defined by $v' = 0$. This yields

$$v \approx v_{sil}(I_{app}) := I_{app}/g_L + v_L, \tag{9.1}$$

which we use below. Now $\tau_h(v)$ tends to an asymptotic value τ_h^- as $v \to -\infty$, and $v_{sil}(I_{app})$ is sufficiently negative for parameters considered such that we can take $\tau_h(v) \approx \tau_h^-$ in the silent phase. Based on (2.4), (4.3), and (4.4), we thus approximate $a \approx 1/\tau_h^-$.

To estimate b and c, note that the function $h_\infty(v)$ is sigmoidal, with horizontal asymptotes at 1 as $v \to -\infty$ and at 0 as $v \to \infty$. Over the transitional region between these asymptotes, $h_\infty(v)$ is approximately linear. Further, since cells with $I = I_{max}$ are oscillatory, it is likely that the v values of cells in the silent phase lie in this transitional region. Thus we derive a least squares linear estimate of $h_\infty(v)$ over this region. Using $v \approx I/g_L + v_L$ in the silent phase from (9.1) converts the approximation of $h_\infty(v)$ into a linear function of I, namely, $BI + C$, which we substitute into (4.4). With this substitution, a comparison of (4.4) and (4.5) yields $b = aB$ and $c = aC$.

For simulation of the nonlinear boundary value problem (6.7), with $h(I_{max}) = h_{RK}$, several additional parameters are needed. We can approximate ρ, which appears in (4.3), as $\rho \approx 1/\tau_h^+$, where τ_h^+ denotes the positive asymptotic value of $\tau_h(v)$. Additionally, we require expressions for $h_{RK}, h_{LK}^{eff}(I)$, and $I_{syn}^u(I)$. The former two can be solved for dynamically at discrete I values (with $I = I_{max}$ for h_{RK}), analogously to the estimation of h_{LK} described above, and the results for $h_{LK}^{eff}(I)$ can be interpolated. A specific form must be assumed for $I_{syn}^u(I)$. Suppose that the I values in the network are distributed uniformly over $[I_{min}, I_{max}]$ and that cells jump down in order of decreasing I, as was the case in our simulations. Then, for $cell(I)$ in the silent phase, $I_{syn}^u(I) \approx g_{syn}(v_{syn} - v_{sil}(I))(I_{max} - I)/(I_{max} - I_{min})$.

Acknowledgments. The authors thank Rob Butera for introducing them to this problem and for input on simulations, and they thank John Rinzel for many helpful discussions.

REFERENCES

[1] J. T. Ariaratnam and S. H. Strogatz, *Phase diagram for the Winfree model of coupled nonlinear oscillators*, Phys. Rev. Lett., 86 (2001), pp. 4278–4281.

[2] R. Butera, J. Rinzel, and J. Smith, *Models of respiratory rhythm generation in the pre-Bötzinger complex.* I. *Bursting pacemaker neurons*, J. Neurophysiology, 81 (1999), pp. 382–397.

[3] R. Butera, J. Rinzel, and J. Smith, *Models of respiratory rhythm generation in the pre-Bötzinger complex.* II. *Populations of coupled pacemaker neurons*, J. Neurophysiology, 81 (1999), pp. 398–415.

[4] C. C. Chow, *Phaselocking in weakly heterogeneous neuronal networks*, Phys. D, 118 (1998), pp. 343–370.

[5] G. de Vries and A. Sherman, *From spikers to bursters via coupling: Help from heterogeneity*, Bull. Math. Biol., 63 (2002), pp. 371–391.

[6] C. DelNegro, S. Johnson, R. Butera, and J. Smith, *Models of respiratory rhythm generation in the pre-Bötzinger complex.* III. *Experimental tests of model predictions*, J. Neurophysiology, 86 (2001), pp. 59–74.

[7] C. DelNegro, C. Wilson, R. Butera, H. Rigatto, and J. Smith, *Periodicity, mixed-mode oscillations, and quasiperiodicity in a rhythm-generating neural network*, Biophys. J., 82 (2002), pp. 206–214.

[8] G. B. Ermentrout, *Simulating, Analyzing, and Animating Dynamical Systems: A Guide to XPPAUT for Researchers and Students*, Software Environ. Tools 14, SIAM, Philadelphia, 2002.

[9] G. B. Ermentrout and N. Kopell, *Frequency plateaus in a chain of weakly coupled oscillators*, SIAM J. Math. Anal., 15 (1984), pp. 215–237.

[10] D. Golomb and J. Rinzel, *Dynamics of globally coupled inhibitory neurons with heterogeneity*, Phys. Rev. E (3), 48 (1993), pp. 4810–4814.
[11] D. Golomb, X.-J. Wang, and J. Rinzel, *Synchronization properties of spindle oscillations in a thalamic reticular nucleus model*, J. Neurophysiology, 72 (1994), pp. 1109–1126.
[12] S. Johnson, J. Smith, G. Funk, and J. Feldman, *Pacemaker behavior of respiratory neurons in medullary slices from neonatal rat*, J. Neurophysiology, 72 (1994), pp. 2598–2608.
[13] N. Kopell and G. B. Ermentrout, *Mechanisms of phase-locking and frequency control in pairs of coupled neural oscillators*, in Handbook of Dynamical Systems, Vol. 2: Towards Applications, B. Fiedler ed., North–Holland, Amsterdam, 2002, pp. 3–54.
[14] N. Koshiya and J. Smith, *Neuronal pacemaker for breathing visualized in vitro*, Nature, 400 (1999), pp. 360–363.
[15] Y. Kuramoto, *Chemical Oscillations, Waves, and Turbulence*, Springer-Verlag, Berlin, 1984.
[16] J. Rubin and D. Terman, *Geometric singular perturbation analysis of neuronal dynamics*, in Handbook of Dynamical Systems, Vol. 2: Towards Applications, B. Fiedler ed., North–Holland, Amsterdam, 2002, pp. 93–146.
[17] J. Smith, H. Ellengerger, K. Ballanyi, D. Richter, and J. Feldman, *Pre-Bötzinger complex: A brainstem region that may generate respiratory rhythm in mammals*, Science, 254 (1991), pp. 726–729.
[18] D. Somers and N. Kopell, *Rapid synchronization through fast threshold modulation*, Biol. Cybern., 68 (1993), pp. 393–407.
[19] D. Somers and N. Kopell, *Waves and synchrony in networks of oscillators of relaxation and non-relaxation type*, Phys. D, 89 (1995), pp. 169–183.
[20] D. Terman and D. L. Wang, *Global competition and local cooperation in a network of neural oscillators*, Phys. D, 81 (1995), pp. 148–176.
[21] J. White, C. C. Chow, J. Ritt, C. Soto, and N. Kopell, *Synchronization and oscillatory dynamics in heterogeneous, mutually inhibited neurons*, J. Comput. Neurosci., 5 (1998), pp. 5–16.
[22] A. Winfree, *Biological rhythms and the behavior of coupled oscillators*, J. Theoret. Biol., 16 (1967), pp. 15–42.